Elastic p-p scattering amplitudes at 6 GeV/c

M. Matsuda
*Department of Physics, Virginia Polytechnic Institute and State University, Blacksburg, Virginia 24061 and Faculty of Integrated Arts and Sciences, Hiroshima University, Hiroshima 730, Japan**

H. Suemitsu
Faculty of Integrated Arts and Sciences, Hiroshima University, Hiroshima 730, Japan

M. Yonezawa
Department of Physics, Hiroshima University, Hiroshima 730, Japan
(Received 10 December 1985)

A phase-shift analysis of the experimental data in elastic p-p scattering at 6 GeV/c has been made. The scattering amplitudes have been almost uniquely determined in the small-$|t|$ region $\lesssim 0.5$ (GeV/c)^2 [$\lesssim 0.8$ (GeV/c)^2 up to the common phase factor]. The present solutions support the results of the fixed-t amplitude analysis of the Argonne group for their gross features.

I. INTRODUCTION

At Argonne National Laboratory (ANL) in the late 1970s, a series of experiments of elastic p-p scattering were performed at the laboratory momentum $P_L = 6$ GeV/c toward the goal of determining the scattering amplitudes. Previously we have obtained two types of solutions by phase-shift analysis of an interim set of experimental data.[1]

Recently double- and triple-spin-correlation-parameter data over the squared-momentum-transfer (t) range between -0.2 and -1.0 (GeV/c)^2 have been published, which have completed the Argonne experiments at $P_L = 6$ GeV/c (Ref. 2). These data constitute the bulk of the presently available spin-correlation data of p-p scattering at 6 GeV/c and give us the expectation for considerable improvement in our knowledge of the p-p scattering amplitudes at this energy. We have now performed a phase-shift analysis (PSA) of the revised data set including these new spin-correlation data.

In the next section we briefly summarize our approach to the PSA, compile the experimental data taken for the PSA, and give its results. In the new Argonne data some of the observables, especially small depolarization D_{LS} at $-t = 0.3$–0.5 (GeV/c)^2 are not reproduced well by the PSA solutions. The end of Sec. II is devoted to the examination of this problem. In Sec. III we show the helicity amplitudes given by the PSA solutions and compare them with the results of the Argonne amplitude analysis. Section IV gives some concluding remarks.

II. PHASE-SHIFT ANALYSIS AND SOLUTIONS

A. Modified phase-shift analysis

A phase-shift analysis (PSA) is a powerful method for the determination of scattering amplitudes, automatically satisfying the partial-wave unitarity constraints. It, through rotation functions, relates the observables at different momentum transfers and fixes the overall common phase factor of the scattering amplitudes. This is a distinct advantage over the fixed-t amplitude analysis. The main weakness is, among others, a difficulty arising from an ever-increasing number of participating partial waves as the energy of the incident particle goes higher. This causes doubts about its feasibility at high energies. Nevertheless, the utility of the PSA of nucleon-nucleon scattering has been demonstrated by several groups[3–6] in the dibaryon region of a few GeV/c.

In order to decrease the number of free parameters in the PSA of N-N scattering at high energies, one can use the one-boson-exchange (OBE) amplitudes for the peripheral part of N-N scattering amplitudes instead of the one-pion-exchange (OPE) amplitude used in the modified PSA at low energies,[7] in view of the success of the OBE model.[8] The OBE amplitudes, however, have energy and momentum-transfer dependences quite different from the ones used at low energies due to Reggeization effects.

To cope with this point, we use an OBE-type amplitude[9] which essentially varies the s and t dependences of the OBE amplitude, and carry out a kind of modified PSA. The scattering amplitude is schematically now expressed as follows:

$$M = \sum_{J<J_0} [f_J(\delta_J,\eta_J)] + \sum_{J_0\le J<J_1} [f_J(\delta_J(\mathrm{OBE}),\eta_J)] + M_{\mathrm{OBE}}(J\ge J_1)\ . \quad (1)$$

Here $[f_J]$ denotes the contribution from the partial-wave amplitude f_J of angular momentum J. [We use the parametrization by the nuclear-bar phase shift δ_J and the reflection parameter η_J (Ref. 10).] The boundary angular momentum J_0 and J_1 are chosen by their corresponding impact parameter b equal to about 1.0 and 2.5 fm, respectively. The lower angular momentum states with $J<J_0$ in the first term are completely free in the data fitting. In the second term the phase shifts δ_J(OBE) for the waves

TABLE I. The list of experimental data used in the present analysis.

Observable	Momentum	$-t$ range [(GeV/c)^2]	Number	Laboratory	Reference
σ_t			1	CERN	GI(69)
σ_{el}			1	ANL	AM(74)
$\Delta\sigma_T$			1	ANL	BO(74)
$\Delta\sigma_L$			1	ANL	AU(77)
α			1	CERN	GI(69)
$\mathrm{Re}F_2$			1		GR(78)
$\mathrm{Re}F_3$			1		GR(78)
$d\sigma/dt$		4.8	1	LBL	CL(66)
		4.8	1	ANL	AK(67)
	6.07	1.1–4.7	3	LRL	AN(68)
	6.07	1.2–4.7	11	LRL	AN(68)
		0.0–1.9	40	ANL	AM(74)
		2.7–4.8	22	ANL	JE(77)
P		0.5–2.0	8	ANL	OF(74)
		0.5–2.8	11	ANL	FE(74)
		0.0–0.5	16	ANL	RU(75)
		0.1–1.8	17	ANL	MI(77)
		0.0–0.4	11	ANL	KL(77)
		0.6–1.1	3	ANL	RA(77)
		0.5–1.1	4	ANL	BO(78)
		0.5	1	ANL	BO(78),FE(74)
(C_{3n})		0.5–1.1	4	ANL	BO(78)
		0.9–1.1	2	ANL	CR(79)
D_{NN}		0.3	1	CERN	DE(73)
		0.5	1	ANL	FE(74)
		0.3–1.7	7	ANL	AB(75)
		0.6–1.1	3	ANL	RA(77)
		0.5	1	ANL	BO(78)
$D_{SS'}$		0.2–0.5	7	CERN	DE(73)
$D_{SL'}$		0.3	1	CERN	DE(73)
D_{SS}		0.3–1.0	6	ANL	AU(85)
D_{SL}		0.3–0.7	4	ANL	AU(85)
D_{LL}		0.3–0.7	4	ANL	AU(85)
D_{LS}		0.3–0.7	4	ANL	AU(85)
A_{NN}		0.5–2.8	11	ANL	FE(74)
		0.1–1.4	10	ANL	HI(75)
		0.1–1.8	17	ANL	MI(77)
		0.6–1.1	3	ANL	RA(77)
		0.5	1	ANL	BO(78)
		0.9–1.1	2	ANL	CR(79)
		2.5–4.8	7	ANL	CR(81)
A_{SS}		0.0–1.5	22	ANL	AU(76)
A_{LL}		0.1–0.9	13	ANL	AU(77)
		0.5–3.6	14	ANL	WI(78)
A_{SL}		0.5–3.6	14	ANL	WI(78)
		0.5–3.6	11	ANL	SW(77)
K_{LS}		0.3–0.7	4	ANL	AU(85)
K_{NN}		0.5	1	ANL	FE(74)
		0.6–1.1	3	ANL	RA(77)
		0.5	1	ANL	BO(78)
		0.3–1.0	6	ANL	AU(85)
K_{SS}		0.3–0.7	4	ANL	AU(85)
K_{SL}		0.3–0.7	4	ANL	AU(85)
K_{LL}		0.3–0.7	4	ANL	AU(85)
H_{LSN}		0.3–1.0	6	ANL	AU(85)
H_{NSS}		0.3–1.0	6	ANL	AU(85)
$H_{NSL'}$		0.3–1.0	6	ANL	AU(85)
$H_{LNS'}$		0.3–0.7	4	ANL	AU(85)
$H_{LLN'}$		0.3–0.7	4	ANL	AU(85)

TABLE I. (*Continued*).

Observable	Momentum	$-t$ range [(GeV/c)^2]	Number	Laboratory	Reference
$H_{SNS'}$		0.3–0.7	4	ANL	AU(85)
$H_{SLN'}$		0.3–0.7	4	ANL	AU(85)

GI(69) G. Giacomelli, Report No. CERN/HERA 69-3, 1969 (unpublished).
AM(74) I. Ambats, *et al.*, Phys. Rev. D **9**, 1179 (1974).
BO(74) W. De'Boer, *et al.*, Phys. Rev. Lett. **34**, 558 (1975).
AU(77) I. P. Auer, *et al.*, Phys. Lett. **70B**, 475 (1977); Phys. Rev. Lett. **41**, 354 (1978).
GR(78) W. Grein, *et al.*, Nucl. Phys. **B137**, 173 (1978).
CL(66) A. R. Clyde, Report No. UCRL-16275, 1966 (unpublished).
AK(67) C. W. Akerlof, *et al.*, Phys. Rev. **159**, 1138 (1967).
AN(68) C. M. Ankenbrandt, *et al.*, Phys. Rev. **170**, 1223 (1968).
JE(77) K. A. Jenkins, *et al.*, Report No. ANL-HEP-PR-77-83, 1977 (unpublished).
OF(74) J. R. O'Fallon, *et al.*, Phys. Rev. Lett. **32**, 77 (1974).
FE(74) R. C. Fernow, *et al.*, Phys. Lett. **52B**, 243 (1974).
RU(75) D. R. Rust, *et al.*, Phys. Lett. **58B**, 114 (1975).
MI(77) D. Miller, *et al.*, Phys. Rev. D **16**, 2016 (1977).
KL(77) R. D. Klem, *et al.*, Phys. Rev. D **15**, 602 (1977).
RA(77) L. G. Ratner, *et al.*, Phys. Rev. D **15**, 604 (1977).
BO(78) M. Borghini, *et al.*, Phys. Rev. D **17**, 24 (1978).
CR(79) D. G. Crabb, Report No. UM HE 79-23, 1979 (unpublished).
DE(73) J. Deregel, *et al.*, Phys. Lett. **43B**, 338 (1973); Nucl. Phys. **B103**, 269 (1976).
AB(75) G. W. Abshire, *et al.*, Phys. Rev. D **12**, 3393 (1975).
AU(85) I. P. Auer, *et al.*, Phys. Rev. D **32**, 1609 (1985).
HI(75) G. Hicks, *et al.*, Phys. Rev. D **12**, 2594 (1975).
CR(81) E. A. Crosbie, *et al.*, Phys. Rev. D **23**, 600 (1981).
AU(76) I. P. Auer, *et al.*, Phys. Rev. Lett. **37**, 1727 (1976).
WI(78) M. Williams, report, 1978 (unpublished); see J. Bystricky and F. Lehar, *Nucleon-Nucleon Scattering Data* (Fachinformationszentrum, Karlsruhe, 1981).
SW(77) J. Swift, report, 1977 (unpublished); see J. Bystricky and F. Lehar, *Nucleon-Nucleon Scattering Data* (Fachinformationszentrum, Karlsruhe, 1981).

$J_0 \le J < J_1$ are given by the OBE-type amplitudes[9] (see the Appendix) with the K-matrix unitarization and are varied collectively through OBE parameters, and their associated reflection parameters are also varied. In the last term, the Born term of the OBE-type amplitudes $M_{\rm OBE}$ is used with unit reflection parameters. We take the OBE-type amplitudes with the simplest ingredients of the low-energy OBE model π, σ, ρ, and ω.[8] At 6 GeV/c, J_0 is 7 and J_1 is about 18. The number of the floating parameters is 64, with 17 δ_J, 37 η_J, and 10 boson parameters.

B. Experimental data

The total number of data points used in the analysis is 488. We have omitted some early polarization experiments since there are several more accurate later experiments, and chosen 386 data as listed in Table I. Here the expressions of observables by the spin directions (beam, target; scattered, recoil) in the laboratory system are $P=(N,0;0,0)=(0,N;0,0)=(0,0;0,N)$, $A_{ij}=(i,j;0,0)$, $D_{i,j}=(i,0;j,0)$, $K_{ij}=(i,0;0,j)$, and $H_{ijk}=(i,j;0,k)$, where i, j, and k denote the three directions of measured spin (N, L, or S) and 0 indicates unpolarized.[2] The forward amplitudes

$$\mathrm{Re}F_2 = P_L\,\mathrm{Re}\phi_2\,|_{t=0}/\sqrt{\pi}$$

and

$$\mathrm{Re}F_3 = P_L\,\mathrm{Re}(\phi_1-\phi_3)\,|_{t=0}/\sqrt{\pi}\,,$$

evaluated by dispersion relations, are also used in the analysis.

A best-fit solution is obtained by varying the free parameters so as to minimize the χ^2 value:

$$\chi^2=\sum_{i,j}[(n_j\theta^{\rm ex}_{i,j}-\theta^{\rm th}_{i,j})/\Delta\theta^{\rm ex}_{i,j}]^2\,, \tag{2}$$

where $\theta^{\rm ex}_{i,j}$ is the experimental datum of observable i for the jth experiment with the experimental error $\Delta\theta^{\rm ex}_{i,j}$ and $\theta^{\rm th}_{i,j}$ is its theoretical value. Here n_j is the normalization parameter assigned to the data of the jth group. In the present analysis, n_j is taken to be 1 except for the differential cross sections measured at the laboratory momentum 6.07 GeV/c by two groups.

C. Solutions

We have started the search by taking the solutions A and B of the previous analysis[1] as the initial values for the variable parameters. These two solutions show completely different helicity structures, even at small momentum transfers, except for the dominance of ϕ_1 and ϕ_3.

TABLE II. Phase-shift solutions. (Imρ_J is assumed to be zero.)

Wave	Solution α (χ^2=462) δ (degree)	η	Solution β (χ^2=464) δ (degree)	η
$^1S_0$	−51.56±0.01	0.5826±0.01	−38.74±0.02	0.6165±0.03
$^3P_0$	−58.99±0.02	0.3541±0.03	−54.38±0.04	0.4649±0.04
$^3P_1$	−55.70±0.02	0.3259±0.02	−45.45±0.02	0.4820±0.03
$^3P_2$	−43.03±0.03	0.2568±0.005	−45.20±0.02	0.3641±0.02
Reρ_2,Imρ_2	−0.0007±0.02	(0.0)	0.0581±0.02	(0.0)
$^1D_2$	−37.90±0.009	0.3781±0.006	−36.72±0.007	0.4690±0.03
$^3F_2$	−34.69±0.01	0.3242±0.005	−29.91±0.02	0.3344±0.01
$^3F_3$	−26.77±0.009	0.3676±0.01	−25.72±0.02	0.3805±0.02
$^3F_4$	−10.39±0.005	0.4114±0.007	−8.194±0.03	0.3486±0.01
Reρ_4,Imρ_4	−0.0164±0.02	(0.0)	0.0025±0.03	(0.0)
$^1G_4$	−9.696±0.004	0.4936±0.004	−10.54±0.009	0.4235±0.02
$^3H_4$	−12.23±0.007	0.5764±0.007	−10.38±0.009	0.5212±0.009
$^3H_5$	−9.958±0.008	0.5669±0.004	−7.806±0.01	0.5532±0.01
$^3H_6$	−1.748±0.002	0.6539±0.005	−1.227±0.005	0.6368±0.01
Reρ_6,Imρ_6	−0.0165±0.01	(0.0)	−0.0200±0.01	(0.0)
$^1I_6$	−3.196±0.002	0.6950±0.004	−1.652±0.01	0.6936±0.01
$^3J_6$	−3.339±0.002	0.7412±0.008	−3.871±0.006	0.7612±0.02
$^3J_7$	−2.768	0.7795±0.004	−4.079	0.7790±0.008
$^3J_8$	0.1433	0.8170±0.005	−0.6457	0.8220±0.005
Reρ_8,Imρ_8	−0.0132	(0.0)	−0.0145	(0.0)
$^1K_8$	0.5983	0.8235±0.004	−0.5330	0.8475±0.008
$^3L_8$	−2.098	0.8763±0.005	−2.067	0.9017±0.01
$^3L_9$	−1.301	0.8748±0.004	−1.832	0.8797±0.006
$^3L_{10}$	0.8423	0.9218±0.004	0.0964	0.9027±0.01
Reρ_{10},Imρ_{10}	−0.0109	(0.0)	−0.0103	(0.0)
$^1(l=10)_{10}$	0.7209	0.9321±0.003	0.3281	0.9235±0.005
$^3(l=11)_{10}$	−0.6562	0.9533±0.005	−0.9143	0.9644±0.01
$^3(l=11)_{11}$	−0.7271	0.9404±0.003	−0.8658	0.9417±0.005
$^3(l=11)_{12}$	0.7833	0.9702±0.004	0.3962	0.9601±0.01
Reρ_{12},Imρ_{12}	−0.0085	(0.0)	−0.0079	(0.0)
$^1(l=12)_{12}$	0.5775	0.9681±0.003	0.5108	0.9784±0.007
$^3(l=13)_{12}$	−0.1464	0.9694±0.004	−0.2897	0.9869±0.004
$^3(l=13)_{13}$	−0.4856	0.9779±0.003	−0.4747	0.9806±0.004
$^3(l=14)_{14}$	0.5669	0.9969±0.003	0.4258	0.9856±0.005
Reρ_{14},Imρ_{14}	−0.0065	(0.0)	−0.0062	(0.0)
$^1(l=14)_{14}$	0.4112	0.9959±0.002	0.4473	0.9896±0.002
$^3(l=15)_{14}$	0.0197	0.9859±0.003	−0.0179	0.9876±0.004
$^3(l=15)_{15}$	−0.3642	0.9928±0.003	−0.3168	0.9900±0.004
$^3(l=15)_{16}$	0.3722	1.0	0.3462	0.9993±0.005
Reρ_{16},Imρ_{16}	−0.0049	(0.0)	−0.0048	(0.0)
$^1(l=16)_{16}$	0.2824	0.9974±0.003	0.3325	0.9956±0.003
$^3(l=17)_{16}$	0.0625	0.9886±0.004	0.0717	0.9929±0.004
$^3(l=17)_{17}$	−0.2872	0.9922±0.003	−0.2446	0.9908±0.005
$^3(l=17)_{18}$	0.2343	1.0	0.2476	0.9984±0.004
Reρ_{18},Imρ_{18}	−0.0038	(0.0)	−0.0037	(0.0)
$^1(l=18)_{18}$	0.1944	1.0	0.2329	0.9965±0.003
$^3(l=19)_{18}$	0.0639	1.0	0.0843	0.9935±0.003

The newly obtained partial-wave parameters of the solutions α and β, obtained, respectively, for A and B, are listed in Table II. The boson parameters are listed in Table III as well as the prediction of forward observables. Here the separation of ρ and ω contributions is made by assuming the ω-tensor coupling constant $f_\omega=0$. All of the pion parameters are fixed at the low-energy values. The coupling constants of solution β are smaller than the ones of solution α and are nearer to the Regge extrapolation of the low-energy ones:

$$g(s)=g(4m_N{}^2)(s/4m_N{}^2)^{\alpha_B(0)-J_B},$$

where $\alpha_B(t)$ and J_B are the Regge trajectory and the spin of a boson, respectively.

Both of the solutions α and β reproduce the experimental data well, as seen in their χ^2 values in Table II. Although the fit of the PSA solutions to the experiments are generally good, there are naturally some exceptions: Notably, the small D_{LS} data at small momentum transfers, the $D_{SS'}$ data at $-t=0.30$, 0.34, and 0.37 (GeV/c)^2 and

TABLE III. Boson parameters and the forward observables.

Boson parameters	Solution α	Solution β
Λ_π (MeV)	(135)	(135)
$\Lambda_\rho=\Lambda_\omega$ (MeV)	541±1	427±5
Λ_σ (MeV)	339±2	307±2
n_π	(1.00)	(1.00)
$n_\rho=n_\omega$	1.01±0.00	6.46±0.7
n_σ	4.40±0.02	6.31±1.0
$G_\pi^2/4\pi$	(14.4)	(14.4)
$G_\rho^2/4\pi$	$(3.265\pm0.005)^2$	$(2.624\pm0.010)^2$
$f_\rho^2/4\pi$	$(1.524\pm0.002)^2$	$(1.260\pm0.007)^2$
$G_\omega^2/4\pi$	$(1.699\pm0.003)^2$	$(1.270\pm0.005)^2$
$g_\sigma^2/4\pi$	$(1.380\pm0.002)^2$	$(1.202\pm0.019)^2$

Forward observables	Experiment	PSA Solution α	PSA Solution β
σ_t (mb)	40.75±0.10	40.72	40.73
σ_r (mb)	29.25±0.51	29.51	29.52
$\Delta\sigma_T$ (mb)	0.35±0.07	0.33	0.34
$\Delta\sigma_L$ (mb)	−1.04±0.09	−1.04	−1.03
$\alpha=(\mathrm{Re}N_0/\mathrm{Im}N_0)_{t=0}$	−0.32±0.06	−0.26	−0.29
$\mathrm{Re}F_2$ (GeV^{-1})	−5.4±0.8	−5.4	−5.4
$\mathrm{Re}F_3$ (GeV^{-1})	3.6±1.0	5.0	5.5

the K_{NN} data around $-t=1$ (GeV/c)^2 are not well reproduced. The D_{LS} data are apparently incompatible with D_{SL} ones at $-t=0.38$ and 0.51 (GeV/c)^2 since $D_{LS}\sim -D_{SL}$ at small momentum transfers. We discuss the D_{LS} problem later. The Argonne K_{NN} data around $-t=1$ (GeV/c)^2 are either very small or weakly negative, which seems somewhat questionable. The $D_{SS'}$ data at $-t=0.30$, 0.34, and 0.37 (GeV/c)^2 are inconsistent with the data at nearby points and also with the D_{SS} data, since $D_{SS'}\approx D_{SS}$ in these t values.

The partial-wave amplitudes of two solutions resemble each other in various features as seen in Table II in spite of the notably different starting points in the parameter space in the χ^2 minimization process. We consider that the gross features of the partial-wave amplitudes are now fixed within ambiguity of order of the difference between the two solutions (about 20% or less for dominant low waves). This is supported by the fact that the present solutions give helicity amplitudes consistent with Argonne's, as will be seen later. We, of course, do not claim that the present solutions have the predictive power at large $|t|$ [say, $|t|>2$ (GeV/c)^2], but the experimental data at large $|t|$, if newly added, will require only minor tuning of the present partial-wave solutions.

The depolarization parameter D_{LS} measured at $-t=0.27$, 0.38, and 0.51 (GeV/c)^2 has the small values 0.621, 0.656, and 0.645, respectively. The D_{LS} at small $|t|$ is represented as

$$D_{LS}\approx\tfrac{1}{2}\sin(\theta_R)(|\phi_1|^2-|\phi_2|^2+|\phi_3|^2-|\phi_4|^2)/(|\phi_1|^2+|\phi_2|^2+|\phi_3|^2+|\phi_4|^2)\,, \tag{3}$$

where θ_R is the laboratory recoil angle. Small D_{LS} requires ϕ_2 and/or ϕ_4 of the magnitude comparable with ϕ_1 and ϕ_3 at these t values. This seems unreasonable since at $t=0$, ϕ_2 is very small and ϕ_4 vanishes. Thus, we expect only a small departure of D_{LS} from unity at small momentum transfers.

Starting from the solution A, we have repeated the analysis, where the weights of D_{LS} data are increased by making their errors to the one-fifth's of their experimental ones and obtained the solution α'. The fit to the D_{LS} data are considerably improved in this solution as seen in Fig. 1, but at the sacrifice of some other observables.

In order to see the mutual consistency among data groups, one can use the renormalization parameters x_j introduced by Arndt[11] as

$$\chi^2=\sum_{i,j}[(\theta_{i,j}^{\mathrm{ex}}-x_j\theta_{i,j}^{\mathrm{th}})/\Delta\theta_{i,j}^{\mathrm{ex}}]^2+\sum_j[(1-x_j)/\Delta x_j^{\mathrm{ex}}]^2\,, \tag{4}$$

where Δx_j^{ex} is the systematic error of the data $\theta_{i,j}^{\mathrm{ex}}$ of observable i given by the jth experiment. Assuming the systematic errors $\Delta x_j^{\mathrm{ex}}=0.05$ for all of the data, the χ^2 of solution α' is 953 with these renormalization factors. The values of renormalization parameters are listed in Table IV. If we classify the data by the departure of the renormalization parameter from unity, H_{NSS}, D_{SS}, D_{SL}, K_{LS}, and H_{LSN} form a group different from D_{LS} and the matching of the D_{LS} with the former is not good.

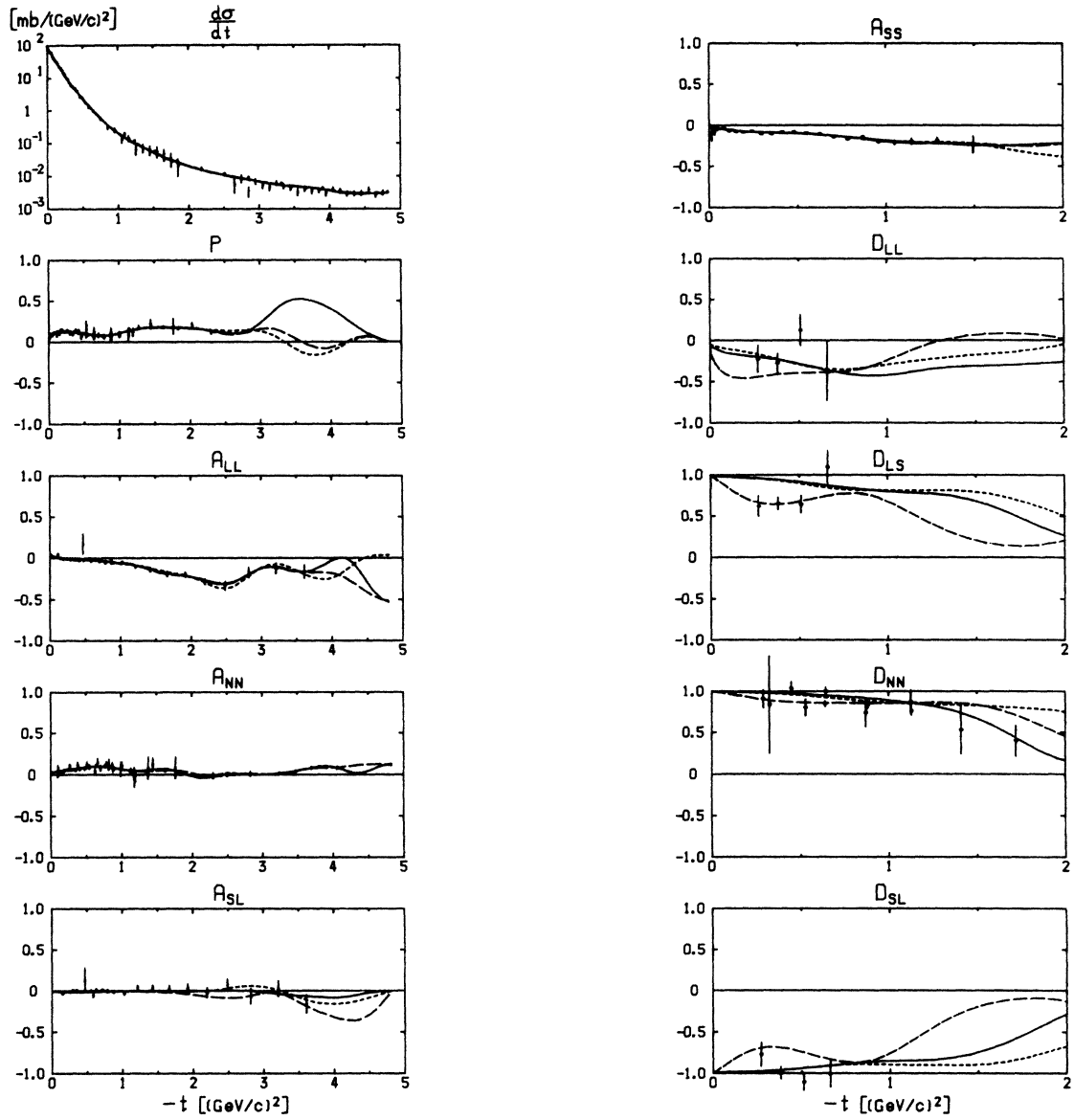

FIG. 1. The experimental data and the predictions by the PSA solutions α, β, and α' which are shown by solid, dotted, and dashed curves, respectively.

III. HELICITY AMPLITUDES

The s-channel helicity amplitudes calculated by the partial-wave solutions and normalized by the square root of the differential cross section are given in Fig. 2. They are rotated by $\arctan(\mathrm{Re}N_0/\mathrm{Im}N_0)$ for comparison with the Argonne amplitude analysis at fixed t which has been carried out assuming a pure imaginary N_0 amplitude.[2]

TABLE IV. The renormalization parameters.

Solution	D_{LS}	D_{SS}	D_{SL}	K_{LS}	H_{NSS}	H_{LSN}
α	0.882	1.004	1.021	1.002	1.001	0.990
α'	1.006	0.707	1.125	0.719	0.649	0.863

Here the s-channel helicity amplitudes[12] are given in standard notation as

$$\phi_1=\langle ++|T|++\rangle,\quad \phi_2=\langle --|T|++\rangle,$$
$$\phi_3=\langle +-|T|+-\rangle,\quad \phi_4=\langle +-|T|-+\rangle,$$

and

$$\phi_5=\langle ++|T|+-\rangle.$$

We compare the s-channel amplitudes rather than the t-channel-exchange amplitudes[13,14] defined as $N_0=(\phi_1+\phi_3)/2$, $N_1=\phi_5$, $N_2=(\phi_4-\phi_2)/2$, $U_0=(\phi_1-\phi_3)/2$, and $U_2=(\phi_2+\phi_4)/2$, since the former shows more interesting structure than the latter in the Argonne solution. Hereafter Re and Im refer, unless mentioned, to the real and

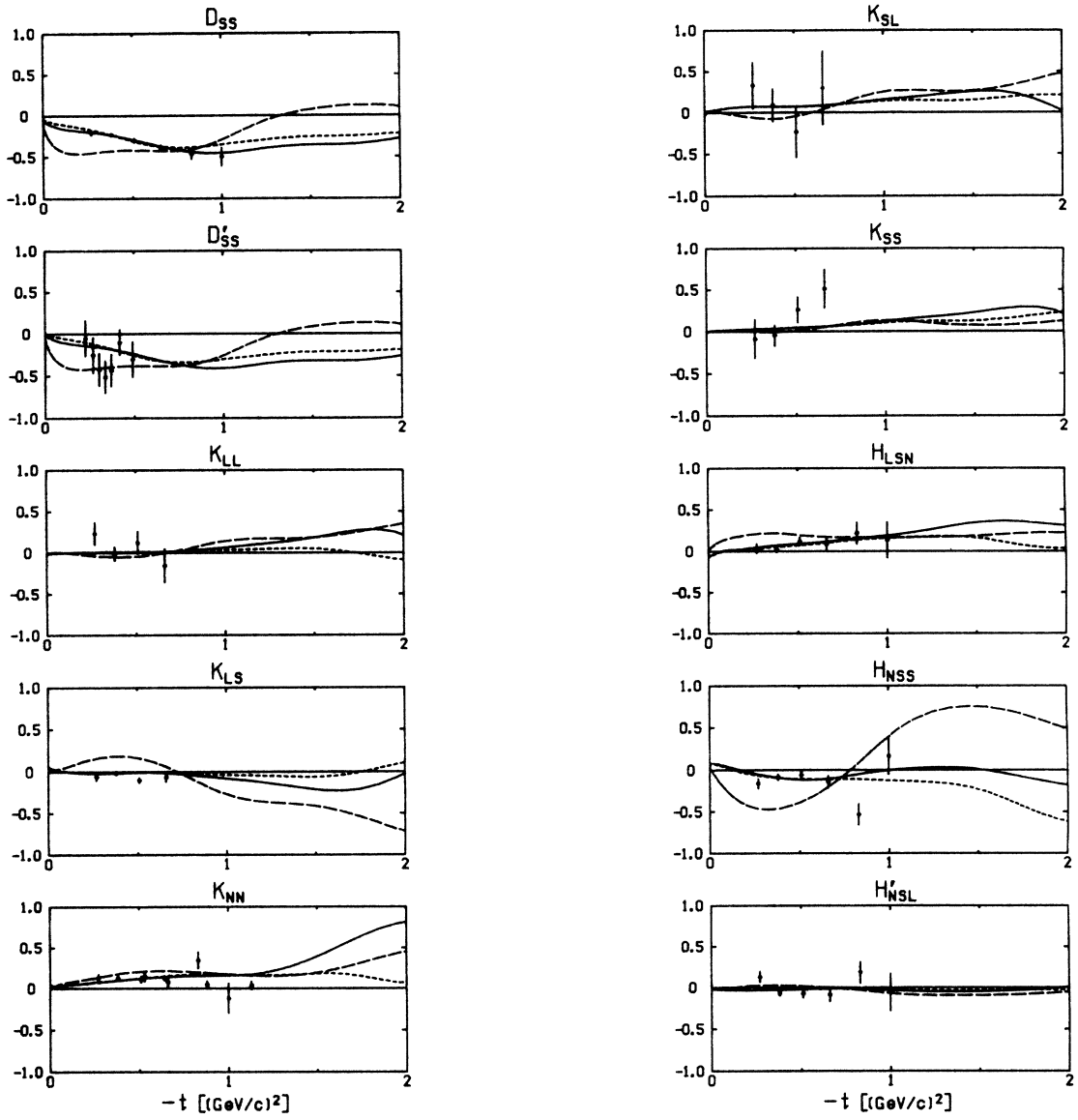

FIG. 1. (*Continued*).

imaginary parts of those rotated helicity amplitudes. The Argonne amplitudes at $-t=0.27$, 0.38, 0.51, 0.66, 0.83, and 1.00 $(\mathrm{GeV}/c)^2$ are also presented in the figures. From these figures, we have found the following features.

(i) In the squared-momentum-transfer region $-t \lesssim 0.8$ $(\mathrm{GeV}/c)^2$, the amplitudes of the solutions α and β agree well with each other and are roughly consistent with the Argonne results. Especially at $-t=0.37$ $(\mathrm{GeV}/c)^2$, where the Argonne analysis shows the least ambiguity, our two solutions fall well within the Argonne bounds. The dominance of the N_0 amplitude, or ϕ_1 and ϕ_3 amplitudes, is well established.

(ii) Our solutions differ from the Argonne results for rapid t variation of $\mathrm{Re}\phi_4$ of the latter. The H_{NSS} data at $-t=0.27$ and 0.83 $(\mathrm{GeV}/c)^2$ might be mainly responsible for the negative $\mathrm{Re}\phi_4$ of the Argonne solution. These H_{NSS} data are, however, deviated significantly from the data at the neighboring points $-t=0.38$, 0.51, and 0.66 $(\mathrm{GeV}/c)^2$ which have smaller error bars. Also the Argonne negative $\mathrm{Re}\phi_2$ at $-t=1.0$ $(\mathrm{GeV}/c)^2$ seems to originate similarly from deviation of the H_{NSS} datum. For this reason the negative $\mathrm{Re}\phi_2$ and $\mathrm{Re}\phi_4$ in the Argonne solution should not be taken seriously.

(iii) The Argonne $\mathrm{Im}\phi_5$ at $-t=1.0$ $(\mathrm{GeV}/c)^2$ has an opposite sign to the ones at smaller $|t|$ and also those of our solutions. Accurate experimental data D_{SS} and D_{SL} will be most helpful to determine $\mathrm{Im}\phi_5$ in this momentum-transfer region.

(iv) In the region $-t>1.5$ $(\mathrm{GeV}/c)^2$, the helicity amplitudes of the solutions α and β differ considerably. Each of the imaginary parts of both unrotated ϕ_1 and ϕ_3 of solution β has a zero around $-t=1.7$ $(\mathrm{GeV}/c)^2$, that reminds us of a diffraction zero which appears in the p-p amplitudes at much higher energies.[15] It is an interesting problem whether or not the diffraction zero is generated already at this energy region. Since the solutions α and β

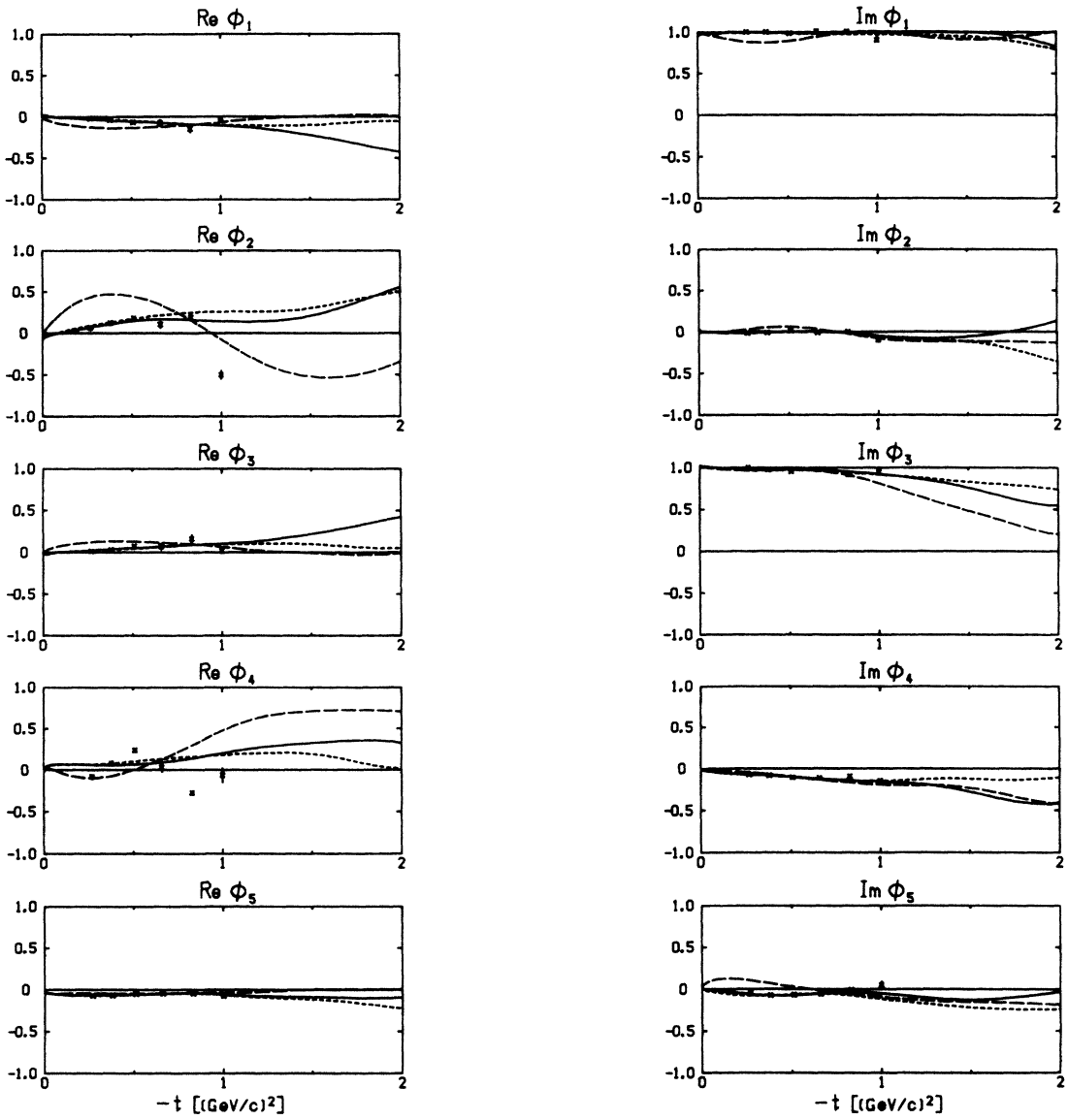

FIG. 2. The rotated helicity amplitudes calculated by the PSA solutions α, β, and α' which are shown by solid, dotted, and dashed curves, respectively. The results of the Argonne fixed-t amplitude analysis are also shown ($\times$).

differ in the appearance of zero in ϕ_1 and ϕ_3 below $-t=2$ (GeV/c)^2, it might be suspected that there would be a drastic change in some observables around $-t=1.7$ (GeV/c)^2 in the β solution. This is, however, not the case, but the two solutions have quite different predictions in this region and future experiments will select one.

IV. CONCLUDING REMARKS

Undoubtedly there will be a herd of partial-wave solutions which covers solutions α and β, and we are still far from the determination of a unique solution. We consider, however, that the correct solution will strongly retain the features common to α and β. The helicity amplitudes at small momentum transfers $|t| \lesssim 0.5$ (GeV/c)^2 [$|t| \lesssim 0.8$ (GeV/c)^2 up to the common phase factor] seem to be nearly fixed. Since the two partial-wave solutions give little difference for the helicity amplitudes in the small-$|t|$ region, the difference in the present partial-wave solutions can be attributed to the uncertainties in the experimental data in the region $|t|>1$ (GeV/c)^2. In this connection it is to be noted that the present data of $d\sigma/dt$ and A_{NN} nearly cover the whole t region and those of P, A_{LL}, and A_{SL} extend over more than half of the available t range, so that some averaged constraints have already been imposed in the present analysis. The present solutions are considered as a reasonable basis for further analyses when large-$|t|$ data become available.

The D_{LS} data measured at ANL are found to be difficult to be reproduced simultaneously with D_{SS}, D_{SL}, K_{LS}, H_{NSS}, and H_{LSN} data by the PSA and require a signifi-

cant change in the structure of amplitudes, especially large and rapidly changing $\mathrm{Re}\phi_2$. A follow-up experiment of D_{LS} is hoped for.

Szwed[16] suggested the importance of the gluon-exchange process with the interchange of interacting quarks in C_{NN} in the large-$|t|$ region beyond 5 $(\mathrm{GeV}/c)^2$ in the explanation of p-p scattering data at 12 GeV/c. The determination of N-N scattering amplitudes covering the full t range in the several-GeV region will be helpful to understand such a picture in more detail and will contribute to understanding strong interactions in the framework of QCD.

ACKNOWLEDGMENTS

The authors wish to thank Professor A. Yokosawa for informing Argonne data before publication and for useful discussions. They are very grateful to Professor R. A. Arndt and Professor L. D. Roper for valuable comments and reading the manuscript. One of the authors (M.M.) thanks Professor R. A. Arndt and Professor L. D. Roper for elucidating data-processing techniques and for warm hospitality during his stay at Virginia Polytechnic Institute and State University.

APPENDIX: MODIFIED PHASE-SHIFT ANALYSIS AT HIGH-ENERGY N-N SCATTERING

The success of the OBE model in low-energy nucleon-nucleon physics[8] suggests a new modified analysis where the peripheral part of the scattering amplitudes is approximated by the one-boson exchange instead of the one-pion exchange in the standard modified analysis. At high energies, the OPE modified analysis is not of much merit since the relative role of the OPE-dominated waves weakens. The OBE amplitudes at high energies, however, are known to change from the low-energy ones due to Reggeization. We, therefore, modify the OBE amplitude by making a replacement:

$$g^2/(m^2-t)\rightarrow\frac{g(s)^2}{m^2}\{\Lambda(s)^2/[\Lambda(s)^2-t/n(s)]\}^{n(s)}\,, \tag{A1}$$

where t is the squared-momentum transfer. The amplitude is normalized to g^2/m^2 at $t=0$ to make easier the comparison of the amplitudes at different energies where m are the observed boson masses. (In the present analysis we take 135 MeV for pion, 770 MeV for ρ and ω mesons, and 400 MeV for σ meson.) The parameter n specifies the behavior at large $|t|$. We note that the modified OBE amplitude tends to $(g^2/m^2)\exp(t/\Lambda^2)$ for $n\rightarrow\infty$. The parameters g, Λ, and n are varied in the PSA as well as the phase shifts (δ,η) of low partial waves. For the partial-wave amplitudes, this modification implies the following replacement of the Legendre function of the second kind appearing in their expressions:

$$Q_J(X_0)\rightarrow\frac{n\Lambda^2}{m^2}(X_0'-1)^n\frac{(-1)^{n-1}}{(n-1)!}Q_J^{(n-1)}(X_0')\,, \tag{A2}$$

$$X_0=1+m^2/2p^2\,, \tag{A3}$$

$$X_0'=1+n\Lambda^2/2p^2\,, \tag{A4}$$

where $Q_J^{(n)}$ is the nth derivative of Q_J and p the center-of-mass-system momentum as well as some appropriate replacement for non-Legendre-function terms.

---

*Permanent address.

[1]M. Matsuda, H. Suemitsu, W. Watari, and M. Yonezawa, Prog. Theor. Phys. **62**, 1436 (1979); **64**, 1344 (1980).

[2]I. P. Auer *et al.*, Phys. Rev. D **32**, 1609 (1985).

[3]N. Hoshizaki, Prog. Theor. Phys. **60**, 1796 (1978); **61**, 129 (1979); K. Hashimoto *et al.*, *ibid.* **64**, 1678 (1980); **64**, 1693 (1980).

[4]R. A. Arndt, quoted in Phys. Rep. **64**, 47 (1980).

[5]M. Akemoto, M. Matsuda, H. Suemitsu, and M. Yonezawa, Prog. Theor. Phys. **67**, 554 (1982).

[6]J. Bystricky, C. Lechanoine-Leluc, and F. Lehar, Report No. DPhPE 82-10, 1984 (unpublished).

[7]P. Cziffra, M. H. MacGregor, M. J. Moravcsik, and H. P. Stapp, Phys. Rev. **114**, 880 (1959).

[8]See, for example, S. Ogawa, S. Sawada, T. Ueda, W. Watari, and M. Yonezawa, Prog. Theor. Phys. Suppl. **39**, 140 (1967).

[9]M. Kawasaki, Y. Susuki, and M. Yonezawa, Prog. Theor. Phys. **47**, 589 (1972).

[10]S. Furuichi, M. Matsuda, and W. Watari, Nuovo Cimento **23A**, 375 (1974).

[11]R. A. Arndt (private communication).

[12]M. L. Goldberger, M. T. Grisaru, S. W. MacDowell, and D. Y. Wong, Phys. Rev. **120**, 2250 (1960).

[13]E. Leader and R. Slansky, Phys. Rev. **148**, 1491 (1966); E. Leader, *ibid.* **166**, 1599 (1968).

[14]F. Halzen and G. H. Thomas, Phys. Rev. D **10**, 344 (1974).

[15]See, for example, T. T. Chou and C. N. Yang, Phys. Rev. **170**, 1597 (1967); Phys. Rev. Lett. **20**, 1213 (1968); T. Maehara, T. Yanagida, and M. Yonezawa, Prog. Theor. Phys. **57**, 1097 (1977).

[16]J. Szwed, Phys. Rev. D **25**, 735 (1982); Phys. Lett. **93B**, 485 (1980).